IJIE

Journal homepage: http://penerbit.uthm.edu.my/ojs/index.php/ijie
ISSN : 2229-838X e-ISSN : 2600-7916

The International Journal of Integrated Engineering

Evaluating The Effect of The Pin's Length to The Strength of Double Sides Friction Stir Welded Aluminum

Djarot B. Darmadi[1*], Annisha Mentary[1], E.M. Yusup[2], S. Mahzan[2]

[1]Mechanical Engineering Department
University of Brawijaya,
MT. Haryono 167, Malang, 65145, INDONESIA

[2]Faculty of Mechanical and Manufacturing Engineering
Universiti Tun Hussein Onn Malaysia
Parit Raja, Batu Pahat, Johor, 86400, MALAYSIA

*Corresponding Author

DOI: https://doi.org/10.30880/ijie.2019.11.05.001
Received 8 January 2019; Accepted 17 April 2019; Available online 10 August 2019

Abstract: Based on previous research, it is believed that the use of double side friction stir welding can improve the obtained joint. It is hoped that a longer pin could broaden the strain hardened area (especially the interference zone) which in turn could produce stronger joints. From tensile test data it can be seen that the tensile strength it is indeed increased by the length of the pin. The maximum tensile strength of 183 MPa was acquired with a pin's length of 6.5 millimeter, which corresponds to a 75% joint efficiency, whilst the lowest efficiency, 42 MPa, was found when the 2.5-millimeter pin was used. The hardness test confirmed the existence of the strain hardening phenomenon, which was shown by the presence of harder materials at interference zone. Other supporting evidence is the micro structure photography. Photos show that the interference zone not only exhibits strain hardening, but also yields a finer dispersed micro structure that provides a stronger joint. A simple Finite Element Simulation was performed to complete and deepen the analysis.

Keywords: double side friction stir welding, strain hardening, pin length

1. Introduction

Aluminum is predicted to replace steel as the most used metals due to its higher strength to weight ratio, environmental friendliness, recyclability with negligible deterioration of mechanical properties and its future prospects as an advanced material. One of the obstacles that has so far prevented a wider usage of aluminum is its low weldability in terms of conventional welding. Since the invention of Friction Stir Welding (FSW) by The Welding Institute (TWI) in 1991, a new hope that FSW could solve the problems with conventional welding when applied to metals with low weldability has arisen.

Some research in FSW has been carried out mainly to join metals with low weldability. Biswas & Kumar evaluated the effects of tool geometry and FSW process parameters applied to commercial aluminum [1]. Their work has shown that tapered pin generally yielded a more ductile joint due to the downward component of centripetal forces. They also found that the rotational speed to feeding speed ratio of 95 rad/mm generated the highest elongation. Raja *et al.* [2] studied the effect of high rotational and feeding speed on the ultimate tensile strength of stir welded AA1100 aluminum alloy. The rotational speed was set at 1500 RPM, 2500 RPM and 3500 RPM with a feeding speed of 10 mm/min, 30 mm/min and 50 mm/min. The highest ultimate tensile strength was measured at 1500 RPM and 50 mm/min with a welding efficiency of about 81%. In the work by Abhishek *et al.*, LM6 aluminum and commercial copper alloys have been joined using FSW [3]. Rotational and feed rate were varied from 400 to 1200 RPM and 20 to 100 mm/min respectively. Some of the parameter variation failed to form a joint, but a 64.81 MPa tensile strength of

*Corresponding author:b_darmadi_djarot@ub.ac.id

Al-Cu could be obtained from the 800 RPM and 60 mm/min combination. Zhang & Wang [4] investigated the change in microstructure due to the FSW process when applied to 6082-T6 aluminum alloy. At the retreating side they observed an evolution of microstructure characterized by lamellar dislocation – formation of subgrain – new recrystallized grain formation and refining of coarse grain. At the advancing side an uneven stress distribution leading to the formation of large and small grain was reported. The intergranular dislocation concentrated in the second phase of Mg_2Si leads to the formation of fractures which made the advancing side the weakest part of the joint. Costa *et al.* [5] studied the lap joint produced by FSW applied to non-heat treatable Al-Mg aluminum (AA5754) and heat treatable Al-Mg-Si aluminum (AA6082). Their results showed that the heat treatable Al-Mg is more susceptible to defect formation which leads to asymmetry in the welds properties. Due to this asymmetry, the normalized yield load (NYL) falls far below one, whilst for the case of non-heat treatable aluminum, where not important welding defects were found, the NYL was almost equal to one. Bayazid *et al.* [6] evaluated the effect of pin profile on the defect formation when FSW was used to join 7075 aluminum alloy. The pin cross section was circular, triangle and square in shape. It is found that the square pin yielded joints with minimal defects. Malik *et al.* [7] studied the effect of various tool pin profiles by means of FEM simulations. They concluded that the square pin consumes less power with no significant changes in temperature. A tapered pin reduces the needed power and decreases the formation of defects. Kalemba-Rec *et al.* [8] investigated the effect of several combination of parameters (such as pin geometry, rotational speeds and alloy configuration) on the resulted joints. It was concluded that straight pins decrease the produced defects and increase the stir zone area. Indeed, increasing the rotational speed on one hand provides the formation of more mixed nugget, but, on the other hand, it may also increase the occurrence of defects, which leads to mechanical properties degradation. Al-moussawi *et al.* developed a FSW model to join DH36 steel [9] which includes temperature model, pressure distribution and material flow. Their model shows that the material flows from the retreating side (where the tangential direction of the tool's movement and the feeding direction are opposed) to the advancing side (where the tangential and the feeding velocities have the same sense). Park *et al.* [10] studied the effect of shoulder diameter in the FSW lap joint. With the higher diameter the stronger joint was obtained due to the wider bound between interfaces. Bozkurt & Boumerzoug [11] - investigated the effect of pin's and shoulder's surface plating on the tensile strength of FSW joints. Their work proved that the surface plating improves the tensile strength.

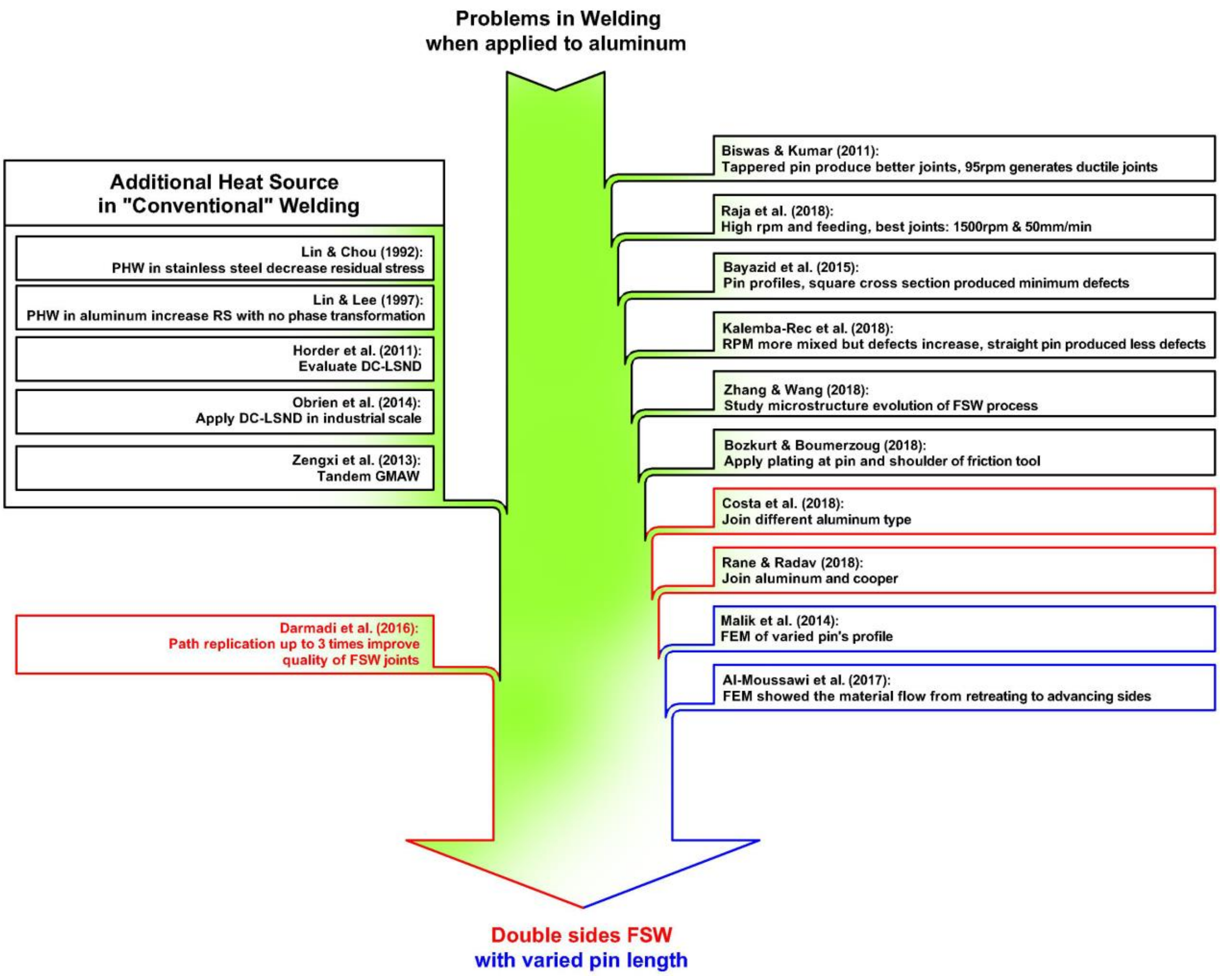

Fig. 1 - The D-FSW Solution.

In other works, an additional heat source has been applied in conventional welding to improve the joint's quality. Lin & Chou [12] have shown that the application of a parallel additional heat source can decrease the residual stress in stainless welding. Lin & Lee [13] applied the PHW (Parallel Heat Welding) to aluminum welding and the residual stress was increased without any change in grain size or the width of HAZ. Horder *et al.* [14] used the DC-LSND (Direct Cooling – Low Stress No Distortion) technique by applying cryogenic CO_2 snow behind the GMAW torch. Their work shows that the DC-LSND decreased the distortion. O'Brien *et al.* [15] applied the DC-LSND in industrial scale with satisfactory results, especially from the joint's distortion point of view. Zengxi *et al.* [16] studied tandem GMAW applied at ship of Australian marine as an alternative to the SAW. It was proven that the T-GMAW joins the metals faster, diminishes the total filler metals, decreases distortion, narrows HAZ and also provides finer microstructures of weld and HAZ. The resulted tensile strength was equal to that obtained by SAW. In a previous publication Djarot *et al*., [17] have shown that a certain number of path repetition (usually 3) can increase the tensile strength because of the strain hardening phenomenon.

In summary existing literature shows that as far as conventional welding is concerned the utilization of additional heat source has been proven to increase the quality of the joint. In the case of FSW, an improved joint strength can be achieved by increasing the number of repetitions due to the strain hardening phenomenon. Based on these findings, this paper investigates the effect of the Double Sides Friction Stir Welding (DS-FSW) pin's length on the resulted joints' quality. The application of the second tool is expected to act as an additional heat source and, at the same time, to provide strain hardening, especially in the interference zone where the pin passes this region twice. The way previous studies and experiments brought to the present research study is shown in Figure 1.

2. Experiment set up

In the experiments performed for the present research a pin with length (the independent variable) of 2.5, 3.5, 5.5 and 6.5 mm has been used. The tools were reproduced from a modification of HSS end mill cutters using turning and grinding machines. All other parameters have been kept constant, namely: rotation speed 1452 RPM, feed rate 24 mm/min and plunged depth followed the length of the pin. The feeding direction has been set to maintain the advancing or retreating sides at the same side of the joined plate. Figure 2 shows the design of the tool which is flat-end cylindrical and Figure 3 describes the resulted joint configuration. As can be seen in Figure 3, in this research the retreating sides were made to be laid at the same section (at the right side). Increasing the pin length means broadening the interference area which, in turn, is hoped to increase the tensile strength of the joint. The FSW was carried out on a Krisbow universal milling machine.

The FSW has been applied to a 7 mm AA7075 Al-Zn aluminum plate. First, the aluminum has been cut in a 15 mm x 25 mm rectangle, then the two resulting aluminum plates have been welded at 25 mm side to form a 30 mm x 25 mm rectangle. First the FSW has been applied to a certain surface and then a second FSW has been applied to the opposite side. The delay time between the first and the second pass was set to be 2 minutes. From this joined rectangle, the tensile specimen shown in Figure 4 was made. The tensile specimen followed AWS standard (shown in Figure 5) and was made by using a milling machine.

The main dependent variable is the ultimate tensile strength of the joint. A quasi static tensile test was carried out and an elongation rate 5mm/minute was measured. The hardness profile, measured by means of an Eseway EW-412AAT micro Vickers tester, is used as a supporting evidence. The evaluated points were taken at the middle section of the weld joint, exactly at the interfaces of the joined plates. Photos of macro and microstructures have also been taken for further results' analysis. A simplified FEM model was finally implemented in order to explain qualitatively the obtained results from an analytic point of view.

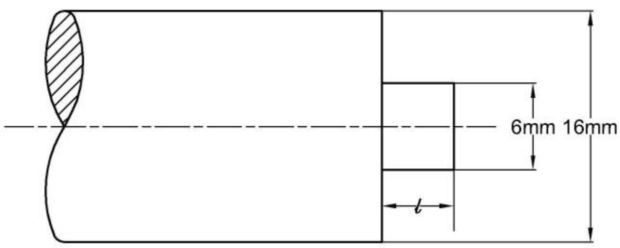

Fig. 2 - The pin design for the FSW tool.

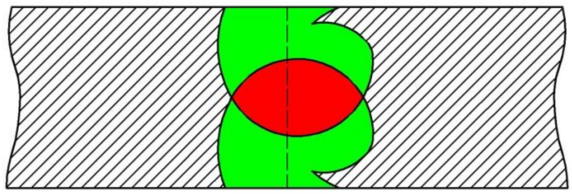

Fig. 3 - The FSW design.

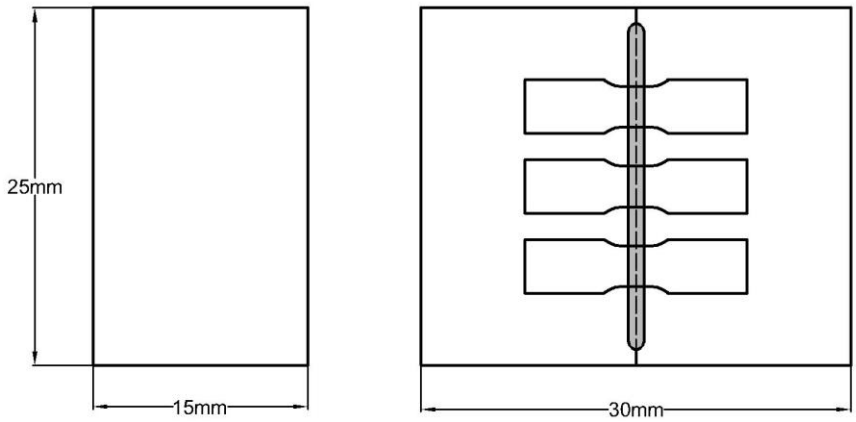

Fig. 4 - The FSW joined plate and the tensile specimen.

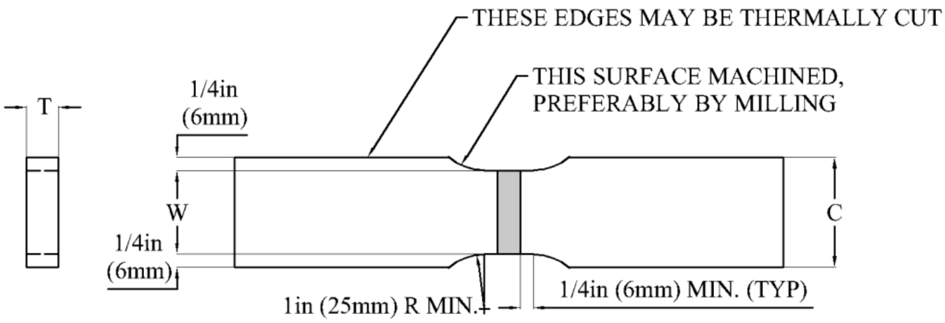

T	W
<1 in (25 mm)	1.50 in±0.01 mm (38 mm±0.25 mm)
≥1 in (25 mm)	1.00 in±0.01 mm (25 mm±0.25 mm)

Fig. 5 - The tensile test specimen.

3. Results and discussions

The major dependent variable (the ultimate tensile strength) as a function of pin's length is shown in Figure 6. From the calculation of tensile test, the tensile strength in MPa of each specimen can be obtained. For each pin's length three data were retrieved. The tensile strength of the base material (244 MPa) has been used for results' normalization and results were also expressed in terms of welding efficiency, as reported on the left axis of Figure 6. From Figure 6 it can be generally concluded that the increasing pin's length improves the tensile strength.

A typical cross section of welded surface is shown in Figure 7, that represents the cross-section macrograph for the 4.5 mm pin's length case. From exam of Figure 7 the five resulting areas of the FSW process can be identified, namely, the Interference Zone (IZ), the Weld Nugget (WN), the Thermo-Mechanically Affected Zone (TMAZ), the Heat Affected Zone (HAZ) and the Base Metal (BM). The left side is always the retreating side and the right side is always the advancing side in spite of where the tool is applied: at top or at the bottom surfaces.

As it has been mentioned in Figure 3, the increasing length of the pin broadens the interference zone. It has been also found that, as previously published in Djarot et al. [17], the repetitions of FSW increases the tensile strength due to strain hardening phenomenon. Hardness profile data have been extracted in order to verify this assumption and they are shown in Figure 8. The data were taken exactly at the previously defined interface border (at the middle of the weld line). In Figure 8 “x” equal to zero means that the data were retrieved from a point exactly at the middle of the plate thickness. On such a coordinate x-axis, a positive (negative) number means that the evaluated point is above (below) the middle point.

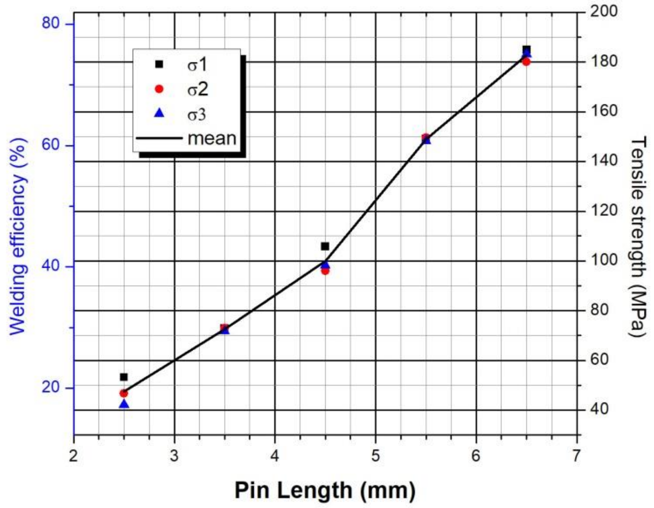

Fig. 6 - The ultimate tensile strength of FSW joint.

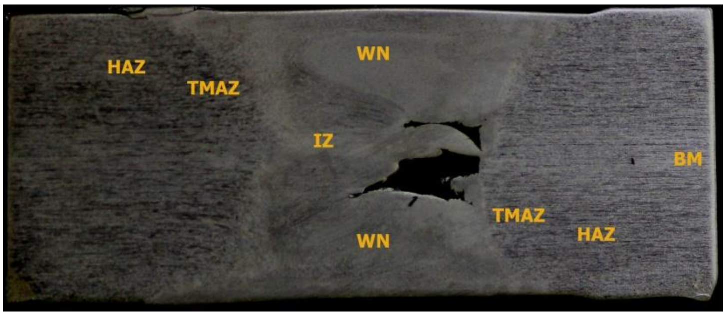

Fig. 7 - The developed macrostructure in DFSW.

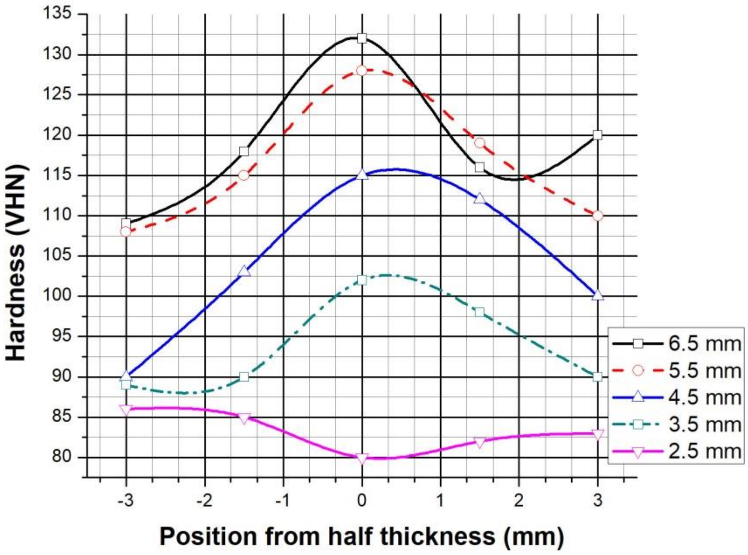

Fig. 8 - Hardness profile for different pin lengths.

It can be seen from Figure 8 that the zero points always have the highest hardness, since they are at the middle of the interference zone. For the pin's length of 2.5 mm there is no interference zone since the thickness of the plate is 7 mm. For the 3.5 mm case, which is exactly half of the plate thickness, the existence of the interference zone can be observed since the weld nugget area, where the plastic strain extensively exists, is a little bit longer than the length of the pin. The existence of this harder material at the interference zone proves the assumption that the strain hardening phenomenon is indeed occurring, especially at the interference zone. Thus, a longer pin not only broadens the interference zone, but also increases the hardness of the evaluated point. And since theoretically the hardness varies linearly with the tensile strength it is plausible to assume that the tensile strength is also a linear function of the pin's length, as it is shown in Figure 6.

The microstructure photos of the base metal, interference zone and upper and lower weld nugget are shown in Figure 9. It can be seen that the nugget and interference zones' structures change from the reference initial base metals micro structure due to both the temperature effects and the mixing force. And it can also be seen that the second strain hardening process produces a finer disperse grain. This appears evident from the exam of the interference zone which shows a finer grain compared to the weld nugget. The existence of this finer grain in turn increases the energy needed to penetrate into the same depth in the hardness test, which confirms the existence of harder material at the interference zone. A finer grain also provides an higher grain boundary resistance energy that gives reason for the higher tensile load.

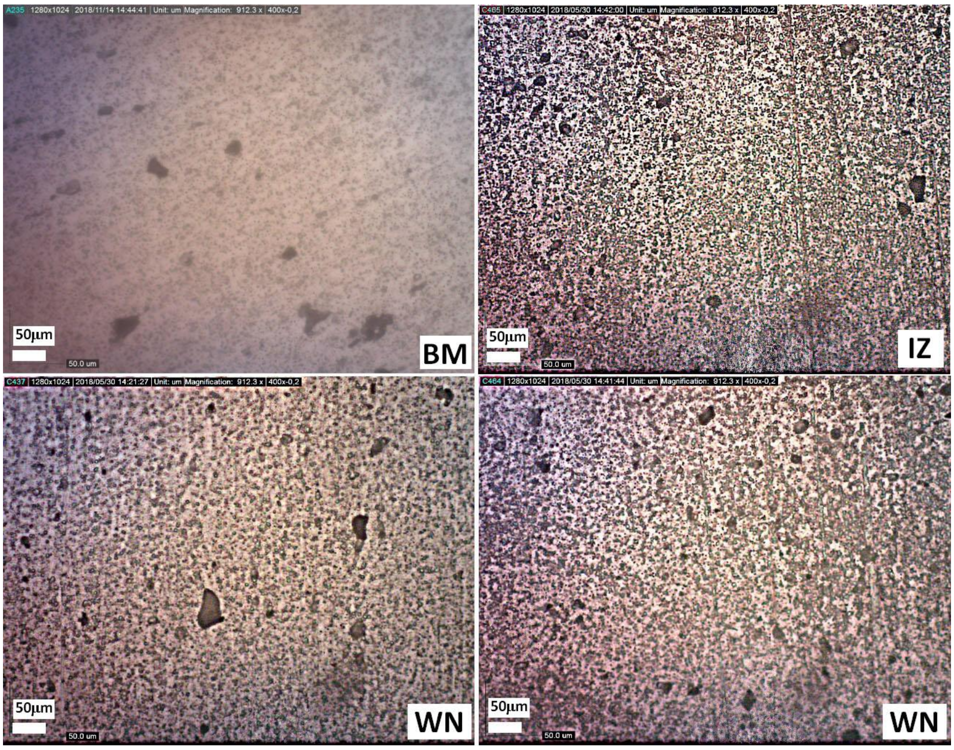

Fig. 9 - The microstructures for 4.5 mm pin: base metal (BM), interference zone (IZ), weld nugget (WN) upper (right) and lower (left).

A FEM simulation was carried out in order to provide a qualitative analytic background. Quantitative accuracy is beyond the scope of this paper. The FEM analysis is applied to the 6.5 mm pin's case, where an extensive interference zone exists, to the 3.5mm pin's case, where the pin's length is equal to half of the plate thickness and finally to the 2.5 mm pin's model where the so called "kissing bond" exists, namely the area where no FSW action takes place at the middle part of the interface. The typical FEM geometric model is shown in Figure 10. The model consists of 11,213 nodes and 55310 elements. A locally refined mesh is used at the interference and the stirred zones. Figure 10 is relative to the 6.5 mm pin model. The drawn areas emulate the regions previously described in Figure 7 that develop when FSW is applied with the further simplifications that the material properties at the interference zone, nugget zone and base metal are defined on the basis of their mean hardness. The load is given in terms of nodal displacement at nodes where the width of the plate is equal to C (equal to 50 mm for this case, see Figure 5) with a displacement rate of 5 mm/minute as in the real quasi static tensile test.

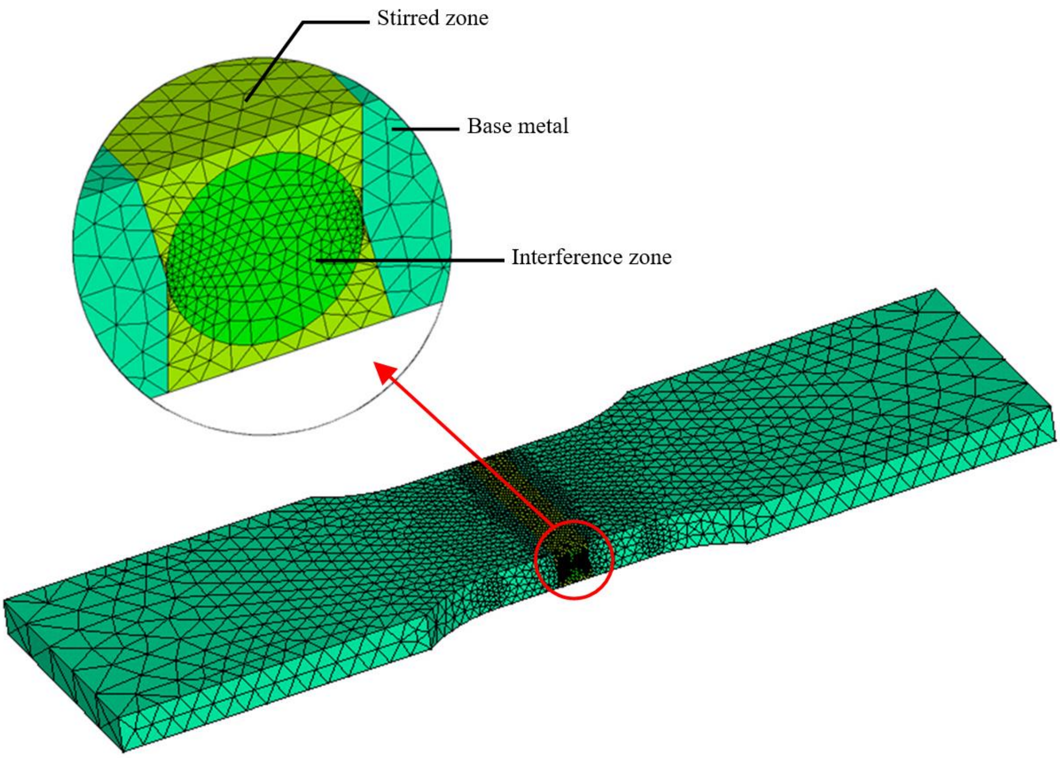

Fig. 10 - The geometric FEM model and mesh of tensile specimen for 6.5 mm pin.

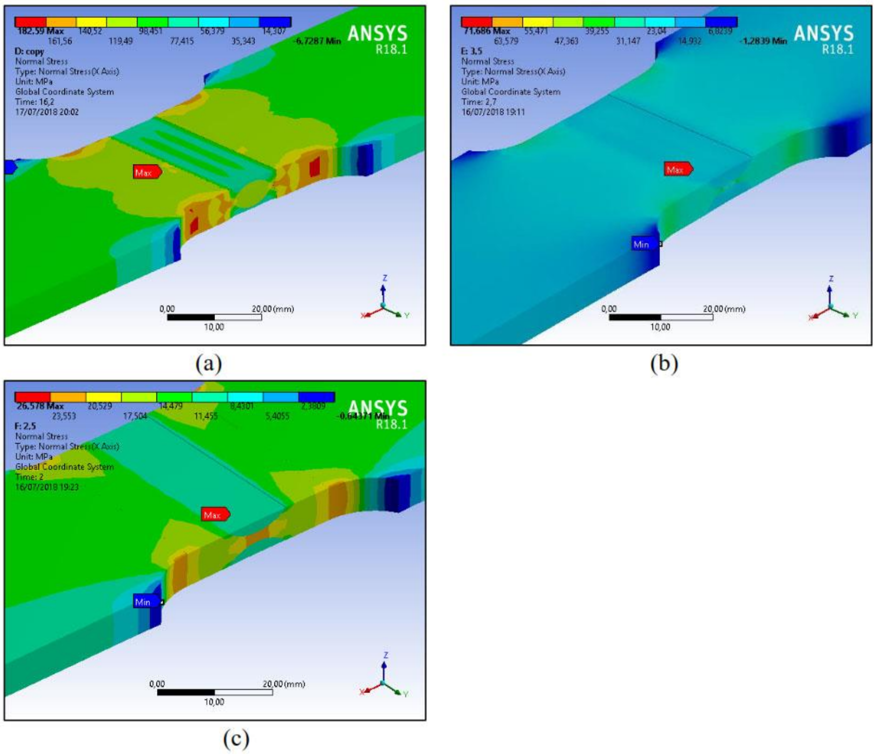

Fig. 11 - Normal stress for pin lengths of (a) 6.5 mm, (b) 3.5 mm and (c) 2.5 mm.

The stress distribution right before ~~the~~ fracture occurs is shown in Figure 13. Before making any comments on Figure 13, it is helpful to briefly examining the comparison of the predicted fracture's structure coming from the FEM analysis with what has been experimentally found. This comparison is offered in Figure 12. Exam of Figure 12 suggests that the FEM model is indeed able to well represent the real physics. The kissing bond can also be well modeled for the pin length case of 2.5 mm. The existence of some differences is deemed understandable due to the simplifications that have been made, especially in terms of material properties and geometry of the weld nugget and interference zones. Moreover, those regions are only represented by single material models, which in itself is far from the real condition. For the 3.5 mm case, no interference region was taken into account for the FEM model. The entire middle cross section is classified as nugget zone. However, for the scope of this research the developed model is considered to be fair enough.

The stress profiles before failure were taken on a path draw through the cross section where the fracture surface takes place. Figure 13 shows the normal stress profile of the 6.5 mm pin's length case along three paths: stress at the middle part, at the top surface and at the bottom surface. It can be seen that the stress at the middle part is generally higher due to the fact that the path is crossing the interference zone at the location where the tensile strength is the highest. The top and the bottom surfaces typically show lower tensile stress values since they are crossing the nugget zone which have lower tensile strength. Stress profiles for bottom and top surfaces show an almost equal trend. Discrepancies may be due to the mesh asymmetry (as shown in Figure 10). In fact, the mesh was generated in an automatic mode, without having a full control on eventual asymmetries created during the automatic grid generation process. Numerical instabilities and a non-perfectly converged solution can give reasons for the non-perfect solution's symmetry between the upper and lower surfaces.

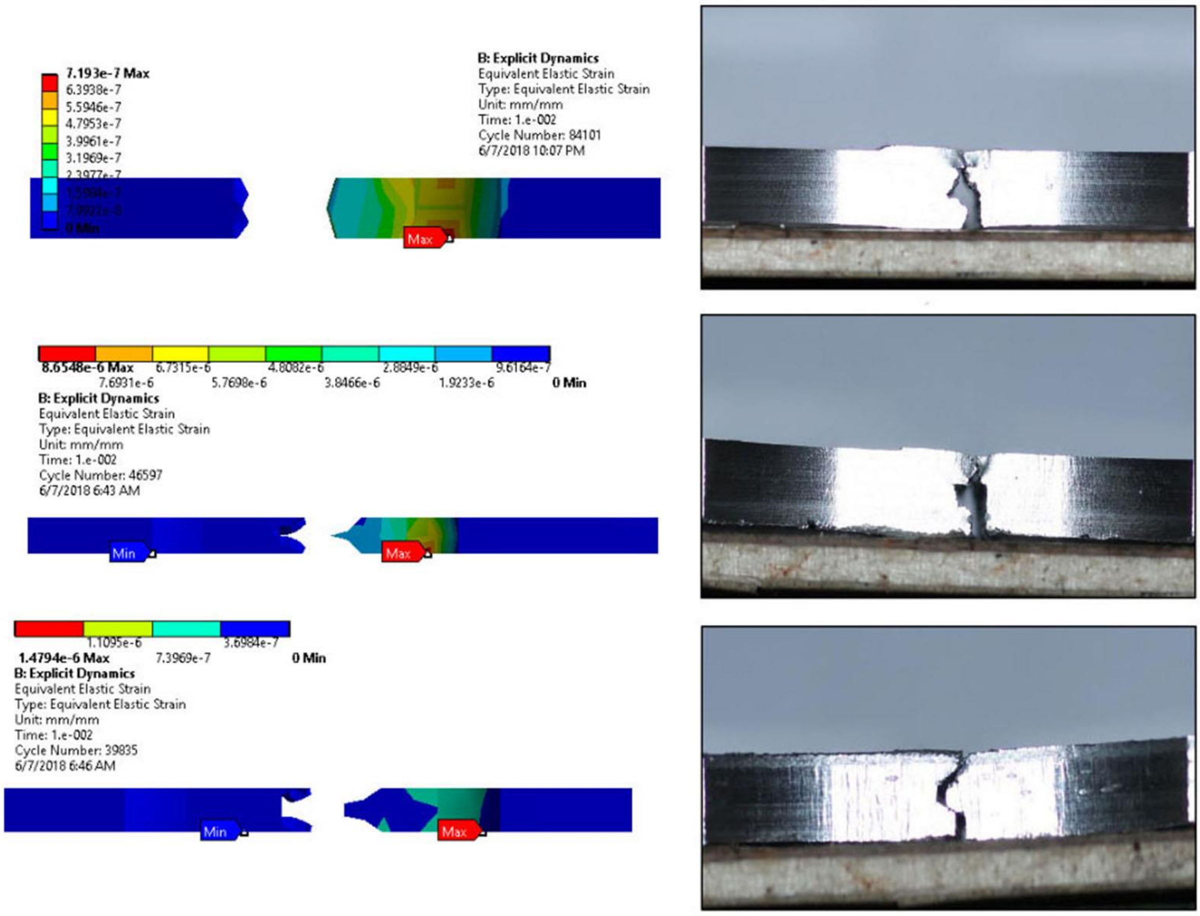

Fig. 12 - Fracture surface of FEM models (left) and experimental results (right) for 6.5 mm (top row), 3.5 mm (mid row) and 2.5 mm (bottom row).

The stress distribution for the 3.5 mm pin model is shown in Figure 14. Just like in the 6.5 mm pin case, the middle path shows higher normal stress since it cut through the interference zone. The normal stress for the 3.5 mm model is lower than that of the corresponding 6.5 mm case due to the different geometric nugget and interference zones' areas. When the interference zone area is bigger, as it is the case in the 6.5 mm model, the total load that can be delivered to the specimen model is higher (note that the load for this FEM model is displacement) and since the stress is the load per unit area, that is why the 6.5 mm model exhibits an higher normal stress profile as shown in Figure 13.

The stress distribution for 2.5 mm pin model is shown in Figure 15. This case is a special one due to the existence of the kissing bond in the middle of the plate. The normal tensile stress in this region is equal to zero, and the observed stress profiles of interest are a little bit shifted to 2.5 mm under the top surface and to 2.5 mm above the bottom surface (at ±1mm according to coordinate system of Figure 8). As in previous models, the middle paths exhibit higher stress profiles compared to the paths drawn through the top and bottom surfaces. Overall the stress profiles show a far lower stress level compared to the 3.5 mm and 6.5 mm models. Again, this is consequence of the fact that the load is given in terms of nodal displacement at the nodes with plate width equal to C. Due to the fact that now the strength of the fracture surface is only represented by the nugget region and the kissing bond, the total force that can be delivered by the joint is the lowest particularly because of the existence of kissing bond. Since the normal tensile stress is the total load divided by the area over which such a force acts (which can be taken to be the cross sectional area W x T in Figure 5), it is understandable that the tensile strength of the joint in the 2.5 mm pin case is the lowest, as it can be seen from the tensile test results shown in Figure 6. It is worth noting here that the tensile strength is actually computed as the applied load divided by the initial (non deformed) cross section area.

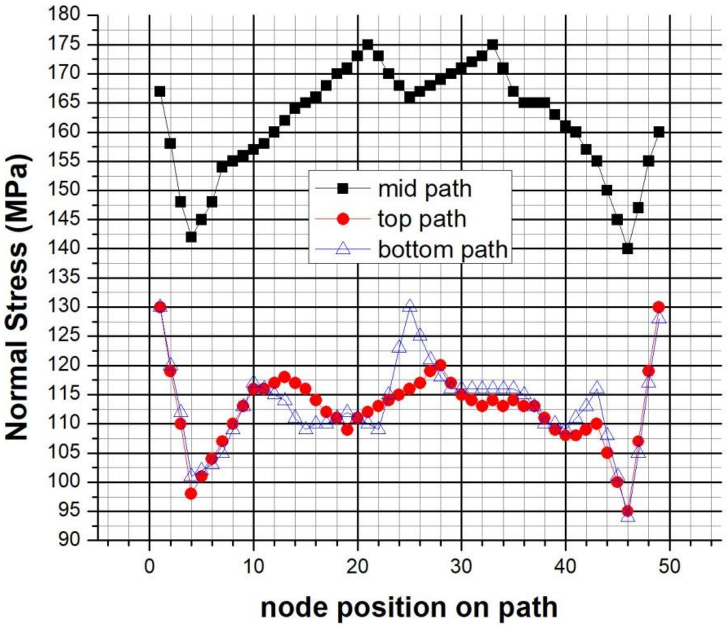

Fig. 13 - Stress profile for the pin length of 6.5 mm.

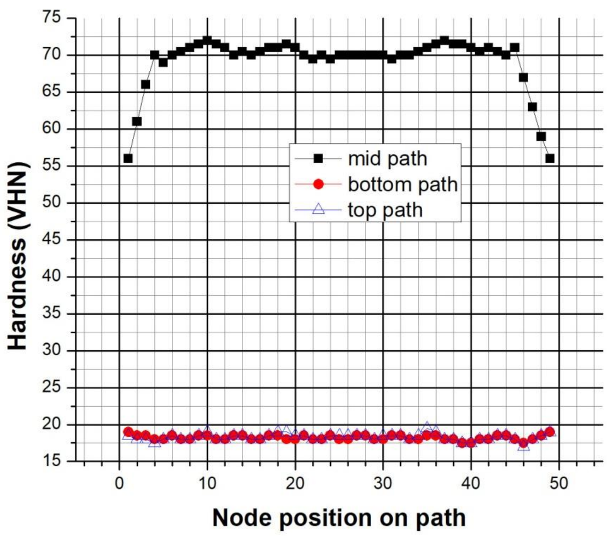

Fig. 14 - Stress profile for the pin length of 3.5 mm.

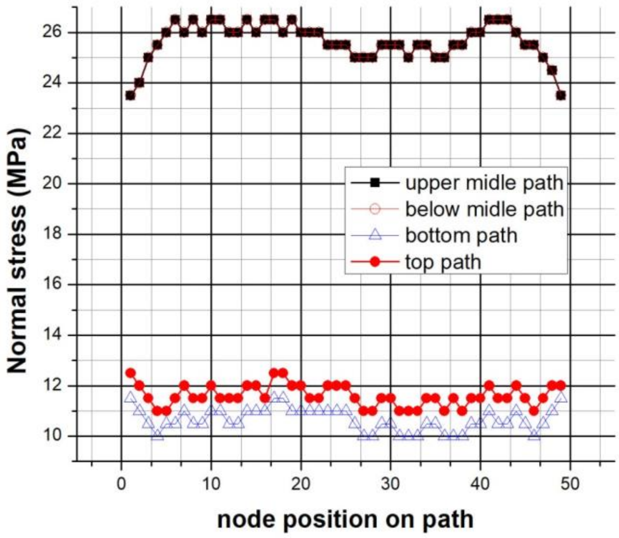

Fig. 15 - Stress profile for the pin length of 2.5 mm.

4. Conclusions

From the discussion above, it can be concluded that the longer pin produces a wider interference zone. Since the interference zone experienced a more extensive strain hardening phenomenon, this region has the highest hardness which translates into the higher tensile strength. The total force that can be borne is the area time the tensile strength, thus the total force is a linear function of the area of the interference zone and of the strength. All of these considerations have been also confirmed by the FEM analysis that emulated the joint condition. Finally, the tensile strength shown in Figure 6 is actually obtained as the maximum load divided by the initial non deformed cross section area and this is why the longer the pin is, the higher the tensile strength will be.

References

[1] Pankaj Biswas and Deepati Anil Kumar (2011). Friction stir welding of aluminum alloy with varying tool geometry and process parameters. Proc. ImechE Vol. 226 Part B: J. Engineering Manufacture, pp. 641 – 648.
[2] P Raja, S Bojanampati, R karthikeyan and R Ganithi (2018). Effect of rotation speed and welding speed on friction stir welding of AA1100 alumnium alloy. IOP Conf. Ser.: Materials Science and Engineering, 346, 012060, pp. 1 – 7.
[3] Abhishek J. Rane and Milind S. Yadav (2018). Effect of friction stir welding process on mechanical and thermal behavior of dissimilar materials. International Journal of Engineering Sciences & Research Technology, vol. 7, no. 4, pp. 420 – 428.
[4] Liangliang Zhang and Xijing Wang (2018). Microstructure evolution and properties of friction stir welding joint for 6082-T6 aluminum alloy. Materials Research. vol. 21, no.6, pp. 1 – 10.
[5] M.I. Costa, C. Leitao and D.M. Rodrigues (2018). Influence of the aluminium alloy type on defects formation in friction stir lap welding of thin sheets. Soldagem & Inspecao, vol. 23, no. 1, pp. 32 – 42.
[6] S.M. Bayazid, H. Farhangi, A. Ghahrarami (2015). Effect of pin profile on defects of friction stir welded 7075 aluminum alloy. Procedia Materials Science, vol. 11, pp. 12-16.
[7] Vinayak Malik, Sanjeev N K, H. Suresh Hebbar and Satish V. Kailas (2014). Investigations on the effect of various tool pin profiles in friction stir welding using finite element simulations. Procedia Engineering, vol. 97, pp. 1060 – 1068.
[8] Izabela Kalemba-Rec, Mateusz Kopyscianski, Damian Miara and Krzysztof Kranowski (2018). Effect of process parameters on mechanical properties of friction stir welded dissimilar 7075-T651 and 5083-H111 aluminum alloys. International Journal of Advanced Manufacturing Technology, vol. 97, pp. 2767 – 2779.
[9] M. Al-moussawi, A.J. Smith, A. Young, S. Cater and M. Faraji (2017). Modelling of friction stir welding of DH36 steel. Int. J. Adv. Manuf. Technol., vol. 1, no. 1, pp. 341 – 360.
[10] Sang-Won Park, Tae-Jin Yoon & Chung-Yun Kang (2017). Effects of the shoulder diameter and weld pitch on the tensile shear load in friction-stir welding of AA6111/AA5023 aluminum alloys. International Journal of Mechanical Engineering and Technology, vol.8, no. 1, pp. 88-99.
[11] Yahya Bozkurt & Zakaria Boumerzoug (2018). Tool material effect on the friction stir butt welding of AA2124-T4 alloy matrix MMC. Journal of Material Research and Technology, vol. 7, no. 1, pp. 29-38.

[12] Y. C. Lin & C. P. Chou (1992). Residual stress due to parallel heat welding in small specimens of type 304 stainless steel. Journal Materials Science and Technology Vol. 8, No. 9, pp. 837-840.
[13] Y.C. Lin. & K.H. Lee (1997). Effect of welding parameters on the residual stress by the parallel heat welding. International Journal of Pressure Vessels and Piping, Volume 71, Issue 2, pp. 197-202.
[14] Holder, R., Larkin, N., Li, H., Kuzmikova, L., Pan, Z. & Norrish, J. (2011). Development of a DC-LSND welding process for GMAW on DH-36 Steel. 56th WTIA annual conference pp. 1-13.
[15] Roger O'Brien, Walter Veldsman & Ahmed Elmarakbi (2014). The development of an industrial robotic low stress no distortion (LSND) welding system. International Institute of Welding, International Welding Congress, New Delhi – India, pp. 164 – 170.
[16] Pan, Zengxi; Larkin, Nathan; Li, Huijun; Van Duin, Stephen; Shen, Chen; Lang, Darren& Sterjovski, Zoran (2013). Evaluation of tandem gas metal arc welding for low distortion butt-welds in naval shipbuilding. Australasian Welding Journal; vol. 58, no. 2, p. 35-41.
[17] Djarot B. Darmadi, Dannar Christyanto and A.A. Sonief (2016). Evaluasi kwalitas sambungan friction stir welding dengan variasi pengulangan lintasan. Proceeding SNTTM XV, Bandung.